# A note on *the secondary load cycle* for a monopile in irregular deep water waves

**Bjørn Hervold Riise[1,2]†, John Grue[1], Atle Jensen[1] and Thomas B. Johannessen[2]**

[1]Department of Mathematics, University of Oslo, Oslo Norway
[2]DNV GL, Oslo, Norway

(Received xx; revised xx; accepted xx)

Laboratory experiments with a bottom hinged surface-piercing cylinder, exposed to irregular deep water waves, are used to investigate high frequency forcing. The focus is on *the secondary load cycle*, a strongly nonlinear phenomenon regarding the wave load on a vertical cylinder, first identified by Grue *et al.* (1993, 1994). For a total of 2166 single wave events the force above $3\omega$ ($\omega$ the governing wave frequency) is used to identify and split the strongly nonlinear forces into two peaks: a high frequency peak closely correlated in time with the wave crest when the total load is positive, and a high frequency peak defining the secondary load cycle which occurs close in time with the wave zero-down-crossing when the total load is negative. The two peaks are studied by regression analysis either as function of the Keulegan-Carpenter number ($KC$), or the Froude number ($Fr$). Regarding the secondary load cycle best correlation is found with $Fr$. The speed of the travelling edge of the undisturbed wave approximates the fluid velocity. A threshold value separating between small and large forces is found for $KC \sim 4-5$, indicating effects of flow separation. Alternatively the threshold occurs for $Fr \sim 0.3-0.4$, indicating local wave effects at the scale of the cylinder diameter. The findings suggest that both effects are present and important.

## 1. Introduction

The high frequency load and response experienced by a monopile exposed to ocean waves are of interest for the renewable industry, where the cylindrical monopile is by far the most popular support structure for wind turbines. With a focus on cost reduction and more optimized design, the industry is seeking improved understanding of the nonlinear wave load mechanisms that are driving high frequency resonance responses (Zhen *et al.* 2015).

The linear wave load, as found for a vertical cylinder by MacCamy & Fuchs (1954), is well defined. Also adequately covered are the nonlinear harmonic forces at $2\omega$ and $3\omega$, where $\omega$ is the fundamental wave frequency. These harmonic forces have been the focus of several previous works. For regular waves, the second harmonic force was analysed by Taylor & Hung (1987); Chau & Eatock Taylor (1992); Newman (1996*b*), while the third harmonic force was analysed by Malenica & Molin (1995); Faltinsen *et al.* (1995). The latter method by Faltinsen, Newman & Vinje, referred to as FNV, is a long wave approximation for deep water. This was later extended to the case of irregular waves by Newman (1996*a*). Recently, Kristiansen & Faltinsen (2017) generalized FNV to finite water depth. For regular waves of moderate wave slope, the theoretical results show good

† Email address for correspondence: bjorn.riise@gmail.com

agreement with measurements, while for steeper waves a discrepancy was observed, indicating important shortcomings for the modelled $3\omega$ force.

The present work investigates the remaining part of the forces, i.e the force contribution above $3\omega$, where more work is needed, particularly for steep waves. This nonlinear force contribution has two main peaks in time domain. The first peak occurs when the wave crest hits the cylinder, when the total load is positive. The second peak occurs between the passage of the wave crest and the following trough, close in time with the zero-down-crossing of the wave, when the total load is negative (see figure 1b and 2). Regarding the first of the two main peaks, we note that wave slamming, due to steep and breaking waves, is strongly correlated in time with the wave crest (Chella *et al.* 2012). The time also correlates with drag forces proportional to the square of the fluid velocity.

The second of the two peaks defines *the secondary load cycle*, a prominent strongly nonlinear phenomenon relating to wave loading on a vertical cylinder, first identified by Grue *et al.* (1993, 1994). The secondary load cycle was further explored by Chaplin *et al.* (1997) in focusing waves and by Grue & Huseby (2002) in the transient part of a regular wave train, and shown by Stansberg (1997) to appear in irregular waves. Several mechanisms have been suggested for the occurrence of the phenomenon. Grue *et al.* (1993, 1994) suggest a resonance between the cylinder and the wave induced flow at the scale of the cylinder diameter, an effect of surface gravity waves governed by the dimensionless Froude number $Fr = U/\sqrt{gd}$, where $U$ is the flow velocity, $g$ the acceleration due to gravity and $d$ the cylinder diameter. The conclusion was based on experiments where the secondary load cycle was observed pronounced for $Fr \sim 0.4$. In a small time interval, the flow experienced by the cylinder may be viewed as a slowly varying horizontal current. The current has a forced wave with wave length $\lambda_C = 2\pi U/g$, and $Fr \sim 0.4$ corresponds to $\lambda_C \sim d$. The wave resistance on a displacement ship, which is considerable for $Fr \sim 0.4$, due to a suction force on the downstream end of the ship, illustrates the strong interaction between the local flow and the geometry at this Froude number.

Rainey (2007) points at local wave breaking on the cylinder. The breaking wave is propagating around the cylinder, leading to the formation of a cavitation bubble at the downstream end. The following collapse of this bubble was suggested as the source of the secondary load cycle. Tromans *et al.* (2006) discussed nonlinear wave scattering as the origin of the high frequency forces. The scattered waves, referred to as *Type I* and *Type II*, were shown by Sheikh & Swan (2005); Swan & Sheikh (2015). *Type I* waves are generated from the run-up and wash-down on the cylinder front and back face. *Type II* scattering is associated with the motion of the free surface around the cylinder. We note that both the nonlinear scattering of waves and the breaking wave shown by Rainey are surface gravity wave effects occurring at the cylinder diameter scale. This supports the role of the Froude number in the analysis of the wave forces.

The more recent developments of Computational Fluid Dynamics (CFD) has made it possible to investigate strongly nonlinear effects by numerical methods. The simulations carried out by Paulsen *et al.* (2014) points to the return flow from the diffracted wave field. When the return flow interacts with the outer flow of the wave motion, a downstream vortex is created. This downstream vortex was suggested as a contribution to the secondary load cycle. For a cylinder exposed to strong waves, Kristiansen & Faltinsen (2017) speculated if flow separation contributes to the high frequency forces. Flow separation is governed by the dimensionless Keulegan-Carpenter number $KC = UT/d$ and $\beta$-number $d^2/\nu T$, where $T$ is the wave period and $\nu$ is the kinematic viscosity. In small scale ($2000 < \beta < 3500$) flow separation may occur already at $KC \approx 1.25$. However, for larger scale, the transition to turbulence suppresses flow separation to larger $KC$ values,

where, for example at $\beta = 11240$ separation is expected to occur at $KC \approx 3$ (Sarpkaya 1986).

Data from a set of laboratory experiments (Riise *et al.* 2018), consisting of six time series with a vertical cylinder exposed to irregular deep water waves, including 2166 single wave events, are here re-analysed with a new perspective. Present work investigates the forces above $3\omega$ with a focus on the secondary load cycle. For each of the single wave events, the high frequency wave-exciting forces, together with the associated local wave parameters, have been considered. While previous work have focused on a limited number of single events, see e.g. Grue & Huseby (2002); Grue (2002), the present analysis enables a systematic study of the phenomenon as a function of wave parameters. The high frequency forces are investigated both as function of $KC$, indicating flow separation effects, and as a function of $Fr$, indicating the effect of surface gravity waves.

Regarding the secondary load cycle, best correlation between the wave parameters and the high frequency forces is found using the speed of the traveling edge of the undisturbed wave to define $Fr$. Furthermore, the findings indicate a threshold value for $KC \sim 4-5$, or alternatively for $Fr \sim 0.3-0.4$. This suggests that both flow separation and the effects of local gravity waves at the scale of the cylinder diameter, are present and important.

The paper is organized as follows: section 2 outlines the methodology and gives an overview of the experiments, section 3 presents and discusses the results, whereas conclusions are presented in section 4.

## 2. Methodology

A total of 2166 single wave events have been found from a set of laboratory experiments, with a cylinder exposed to irregular deep water waves. The experiments, described in §2.1, obtains the wave-exciting moment experienced by the cylinder about the rotation point $z_0$, see figure 1c. The high frequency forces above a harmonic frequency of $3.5\omega_{TT}$, where $\omega_{TT} = 2\pi/T_{TT}$ and $T_{TT}$ is the trough-to-trough period of the local wave , see figure 1a, have been considered for each of the single events. A time window of $\sim 20$ wave periods is used, where a general cut-off is applied at $\omega = 60$ rad/s, which includes the 6th harmonic force for the majority of the waves, i.e. for $T_{TT}\sqrt{g/d} > 8$. The identified high frequency forces clearly include the effects of slamming due to the steep and breaking waves, and also the secondary load cycle.

For a single wave event, $MHF1$ and $MHF2$, are the two most pronounced peaks found from the high frequency part of the wave-exciting moment, see figure 1b. In the figure the high frequency part has been amplified by a factor of five for better visualization. The first peak, denoted by $MHF1$, is found when the total load is positive and associated with the wave crest. The second peak, denoted by $MHF2$, is found when the total load is negative and defines the secondary load cycle. In figure 1b we also define the peak-to-peak moment, $M_{PP}$.

### 2.1. *Experiments*

The experiments (Riise *et al.* 2018) where carried out in the Hydrodynamic laboratory at the University of Oslo in a 25 m long and 0.5 m wide wave flume. The water depth was $h = 0.72$ m. In one end of the tank there is a piston-type of wavemaker which was generating irregular waves. In the opposite end there is a passively absorbing beach.

At a distance of 10.90 m from the wavemaker, a vertical surface-piercing cylinder with a diameter $d = 6$ cm was hinged at a horizontal lateral axis 2 cm above the tank bottom, see figure 1c. The top of the cylinder was connected to load cells (Hottinger Baldwin Messtechnik Type Z6C2 with 10 kg $\hat{=}$ 2 mV/V and 400 Hz sampling rate),

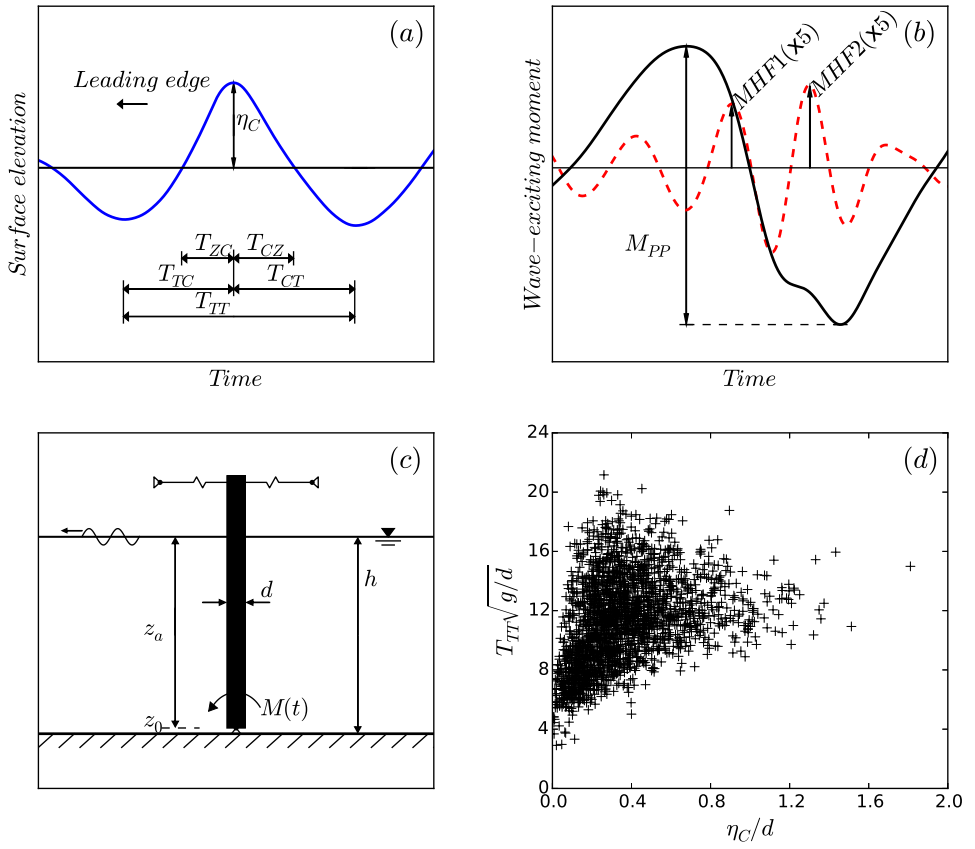


FIGURE 1. *(a)* The crest height $\eta_C$, trough-to-trough period $T_{TT}$, time from trough to crest $T_{TC}$, zero-up-crossing to crest $T_{ZC}$, from crest to trough $T_{CT}$ and crest to zero-down-crossing $T_{CZ}$; *(b)* The peak-to-peak load $M_{PP}$, found from the total measured wave-exciting moment (—), and the high frequency peaks $MHF1$ and $MHF2$, found from the high frequency part (– –) amplified by a factor of 5 ($x5$); *(c)* Cylinder set-up with diameter $d$, water depth $h$, rotation point $z_0$, distance from rotation point to still water level $z_a$ and wave exciting moment $M(t)$; and *(d)* Wave scatter plot with $\eta_C$ and $T_{TT}$ (+).

measuring the force from which the wave-exciting moment $M(t)$ was determined. The accuracy of the load cells is $< 0.01$ Nm, which is $< 3\%$ with regards to the standard deviation of the measured load time series. The undisturbed waves were measured at the cylinder location with the cylinder removed, using ultra sound wave probes (UltraLab ULS Advanced Ultrasound, USS02/HFP with 250 Hz sampling rate). The accuracy of the wave probes is $< 1$ mm, which is $< 2\%$ with regards to the cylinder diameter.

The experimental data consist of six irregular long crested wave time series, each 320 seconds long, based on the JONSWAP spectrum (Hasselmann *et al.* 1973) with peak enhancement factor $\gamma = 3.3$. Each time series was repeated three times, where the median values are used to estimate the various parameters. The standard deviation of the measured crest heights over the three time series is typical 1.5% of the cylinder diameter.

The wave spectral parameters are given in table 1, showing the significant wave height $H_S$, the peak wave period $T_P$ and the normalized peak period $T_P\sqrt{g/d}$, where $g$ is the acceleration due to gravity. These values are used to estimate the spectral

| | 1 | 2 | 3 | 4 | 5 | 6 |
|---|---|---|---|---|---|---|
| $H_S$ [cm] | 5.20 | 6.12 | 6.24 | 6.45 | 7.73 | 9.01 |
| $T_P$ [s] | 0.94 | 0.94 | 1.04 | 1.16 | 1.16 | 1.16 |
| $T_P\sqrt{g/d}$ | 12.0 | 12.0 | 13.3 | 14.8 | 14.8 | 14.8 |

TABLE 1. Spectral wave parameters for the six wave time series. Significant wave height $H_S$, peak wave period $T_P$ and normalized period $T_P\sqrt{g/d}$

steepness $0.5H_Sk_P$, normalized water depth $k_Ph$ and wave length $k_Pr$, where $r$ is the cylinder radius, $k_P$ the peak wave number found using the linear dispersion relation $\omega_P^2 = gk_P \tanh k_Ph$, and $\omega_P = 2\pi/T_P$. This gives moderately to steep waves ($0.10 < 0.5H_Sk_P < 0.14$) in deep water ($2.2 < k_Ph < 3.3$) outside the linear diffraction regime ($0.09 < k_Pr < 0.14$).

For the governing wave frequencies the reflection coefficient, in terms of the amplitude as outlined by Goda & Suzuki (1976), is found to be less than 0.06. A small reflection from the beach primarily affects the force at the fundamental and second harmonic frequency, and to a lesser extent higher harmonic forces ($> 3\omega$, where $\omega$ is the fundamental wave frequency) originating from wave effects at the waterline of the cylinder.

### 2.2. *Wave parameter definitions*

A single wave event is defined by the trough-to-trough period $T_{TT}$ and the crest height $\eta_C$ as shown in figure 1a. The 2166 single wave events are shown in the scatter plot in figure 1d. For later purposes (§3.2) we define the Keulegan-Carpenter number $KC = 2\pi\eta_C/d$, governing for flow separation effects, and the Froude number $Fr = U/\sqrt{gd}$, governing free surface gravity wave effects at cylinder diameter scale. The flow velocity amplitude may be approximated by $U = 2\pi\eta_C/T$, where $T$ is the wave period. Furthermore we define *the leading wave edge*, from trough to crest with the timing $T_{TC}$, or from zero-up-crossing to crest with $T_{ZC}$. We also define *the travelling wave edge*, from crest to trough with $T_{CT}$, or from crest to zero-down-crossing with $T_{CZ}$. In §3.2 we relate the speed of the leading and travelling wave edges of the undisturbed wave to the flow velocity and Froude number. For this an approximation of $U$ is suggested by $U = 2\pi\eta_C/T_i$, which gives $Fr = 2\pi\eta_C/T_i\sqrt{gd}$, where $T_i$ is given by $2T_{TC}$, $4T_{ZC}$, $2T_{CT}$, or $4T_{CZ}$.

## 3. Results

We first illustrate the surface elevation and the wave-exciting moment for four typical wave events, see figure 2. The surface elevation $\eta$ is normalized by the cylinder diameter $d$. The wave-exciting moment $M$ is normalized by $\rho g z_a d^3$, where $\rho$ is the density of water, $g$ the acceleration due to gravity and $z_a$ the distance from the point of rotation to still water level. The time $t$ is normalized by $\sqrt{g/d}$. In the following, $^*$ denotes dimensionless values, i.e. $\eta^* = \eta/d$, $M^* = M/\rho g z_a d^3$ and $t^* = t\sqrt{g/d}$.

In the first event (figure 2a), with a crest height of $\eta_C^* = 1.3$ and a wave period of $T_{TT}^* = 10.4$, we observe evidence of slamming due to the steep wave event. The maximum load has a value of $M^* = 1.1$ and occurs approximately simultaneously with the wave crest. The minimum load has a value $M^* = -1.0$ and occurs between the wave zero-down-crossing and the following trough. This gives a peak-to-peak load $M_{PP}^* = 2.1$ and a time of $t^* = 3.8$ between the maximum and minimum load peaks.

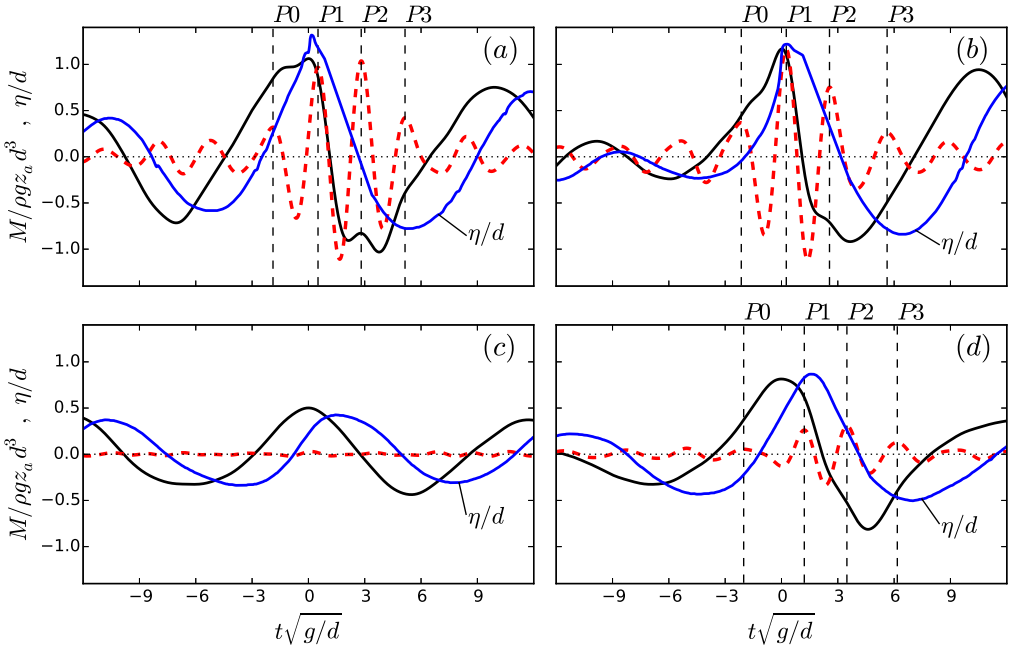


FIGURE 2. Surface elevation (—), total measured wave-exciting moment (—) and high frequency forces amplified by a factor of five (– –) for: *(a)* Series 1, with $(H_S, T_P) = (5.20\text{ cm}, 0.94\text{ s})$, at $t = 250.1$ s; *(b)* Series 3, with $(H_S, T_P) = (6.24\text{ cm}, 1.04\text{ s})$, at $t = 155.7$ s; *(c)* Series 1, with $(H_S, T_P) = (5.20\text{ cm}, 0.94\text{ s})$, at $t = 238.7$ s; and *(d)* Series 3, with $(H_S, T_P) = (6.24\text{ cm}, 1.04\text{ s})$, at $t = 219.8$ s.

The high frequency part of the wave-exciting moment, occurring during the local period of the load history (for $-4.5 < t^* < 6.4$), consist of four peaks. The first peak (P0) is small. This occurs at $t^* = -2.0$ and is close in time with the wave zero-up-crossing, where large inertia forces occur. The second peak (P1) is large, of $MHF1^* = 0.19$, and occurs at $t^* = 0.4$ when the total load is positive. This is closely correlated in time with the wave crest, where large orbital velocity and wave breaking at the column occur. The third peak (P2) is also large, of $MHF2^* = 0.20$, occurring at $t^* = 2.8$ when the total load is negative. This is associated with the secondary load cycle. The last peak (P3), which is small, occurring at $t^* = 5.1$, is close in time with the wave trough.

In the second event (figure 2b), where $\eta_C^* = 1.2$ and $T_{TT}^* = 11.0$, we observe evidence of slamming due to the breaking wave. The maximum load has a value of $M^* = 1.2$ and the minimum load has a value of $M^* = -0.9$. This gives $M_{PP}^* = 2.1$ and $t^* = 3.6$ between the extremes. The same distinct high frequency peaks are observed with $MHF1^* = 0.23$ at P1 and $MHF2^* = 0.15$ at P2.

Considering $MHF1^*$ and $MHF2^*$ for the two events (figures 2a and 2b), the time in between the peaks is $t^* = 2.3$ and the magnitude is $7 - 11\%$ relative to $M_{PP}^*$. In the first event $MHF2^*$ is slightly larger than $MHF1^*$, while in the second event $MHF1^*$ is the largest. From the two events it is found that the first of the two dominant peaks, $MHF1^*$, occurs for $0 < t^* < 1$ (relative to the time of the maximum load), simultaneous to, or shortly after the passing of the wave crest, when the total load is positive. Large orbital velocities and wave slamming due to the steep and breaking waves occur at the cylinder in this time range. The secondary load cycle, $MHF2^*$, occurs for $2 < t^* < 3$.

This is approximately at the same time as for the wave zero-down-crossing. The total load is then negative.

A third event with no visible high frequency force, where $MHF1^* \cong MHF2^* \cong 0.01$, is shown in figure 2c. For the fourth event, see figure 2d, we observe small values of $MHF1^* \cong MHF2^* \cong 0.06$. Regarding the secondary load cycle, it is generally observed that this becomes visible in the range $0.06 < MHF2^* < 0.10$, and is significant for $MHF2^* > 0.10$.

In a resonant build up of the motion response, a set of succeeding load cycles will amplify the response. As an illustration of the importance of the secondary load cycle, we may consider the time varying response $\xi(t)$ of an undamped oscillator exposed to a harmonic force $\cos(\omega_o t)$, with $\omega_0$ the resonance frequency of the oscillator, expressed by the equation of motion $\ddot{\xi}(t) + \omega_0^2 \xi(t) = \alpha_0 \cos(\omega_o t)$. With a start from rest, the response increases according to $\xi(t) \propto t \sin(\omega_0 t)$. This shows that through one load cycle, the response is amplified by a factor equal to $t = 2\pi/\omega_0$, and that both the first and the second of the two large high frequency peaks, $MHF1^*$ and $MHF2^*$, are important.

### 3.1. *Magnitude and period of the secondary load cycle*

In the following we consider the high frequency force contributions for all of the 2166 events. The figures 3a and 3b present the magnitude and timing of the secondary load cycle $MHF2^*$ relative to the total load $M^*_{PP}$. The magnitude ratio $MHF2/M_{PP}$, as shown in figure 3a, increases with regards to $MHF2^*$, clearly indicating the nonlinear behaviour for the high frequency force.

Furthermore, we observe that the magnitude for the large events ($MHF2^* > 0.1$) is up to 12% of the peak-to-peak load. This shows that the present results, with the higher harmonic forces extracted from the wave-exciting moment, are comparable to previous published work, where the force ratio is reported. Grue *et al.* (1993, 1994) reported a magnitude up to 11%, Chaplin *et al.* (1997) $8-12\%$ and Grue & Huseby (2002) $10-15\%$.

The timing of $MHF2^*$ with regards to the positive peak of the total load, shown in figure 3b, seems to converge to around one quarter of a wave period. This is in good agreement with the results reported by Grue & Huseby (2002), and generalizes the previous findings obtained in regular waves to the case of irregular waves.

The difference in magnitude between the high frequency force peak close in time with the wave crest, $MHF1^*$ (P1), and the secondary load cycle, $MHF2^*$ (P2), is shown in figure 3c. We observe that for events with small forces ($MHF2^* < 0.15$ and $MHF1^* < 0.15$), it is mostly the forces associated with the secondary load cycle that is the largest, i.e $MHF2^* > MHF1^*$.

When the forces which occur at the same time as the wave crest become large ($MHF1^* > 0.15$), they also become more dominant, and for the largest forces we observe that the peak P1 is larger than the peak P2 ($MHF1^* > MHF2^*$). Observations show that these events include evidence of slamming due to steep and breaking waves. The difference between the magnitude of P1 and P2 is further visualized by two linear curves fitted to the data. The first curve is fitted to events where $MHF2^* < 0.1$ and the second curve is fitted to events where $MHF2^* > 0.1$.

### 3.2. *KC-number vs. gravity effects.*

The effect of flow separation is considered by investigating the forces as function of the Keulegan-Carpenter number $KC$. Figure 3d shows the behaviour of the high frequency force peak (P1) close in time with the wave crest, $MHF1^*$. The ensemble mean and standard deviation is found together with the second and third order curves $\alpha_2 x^2$ and

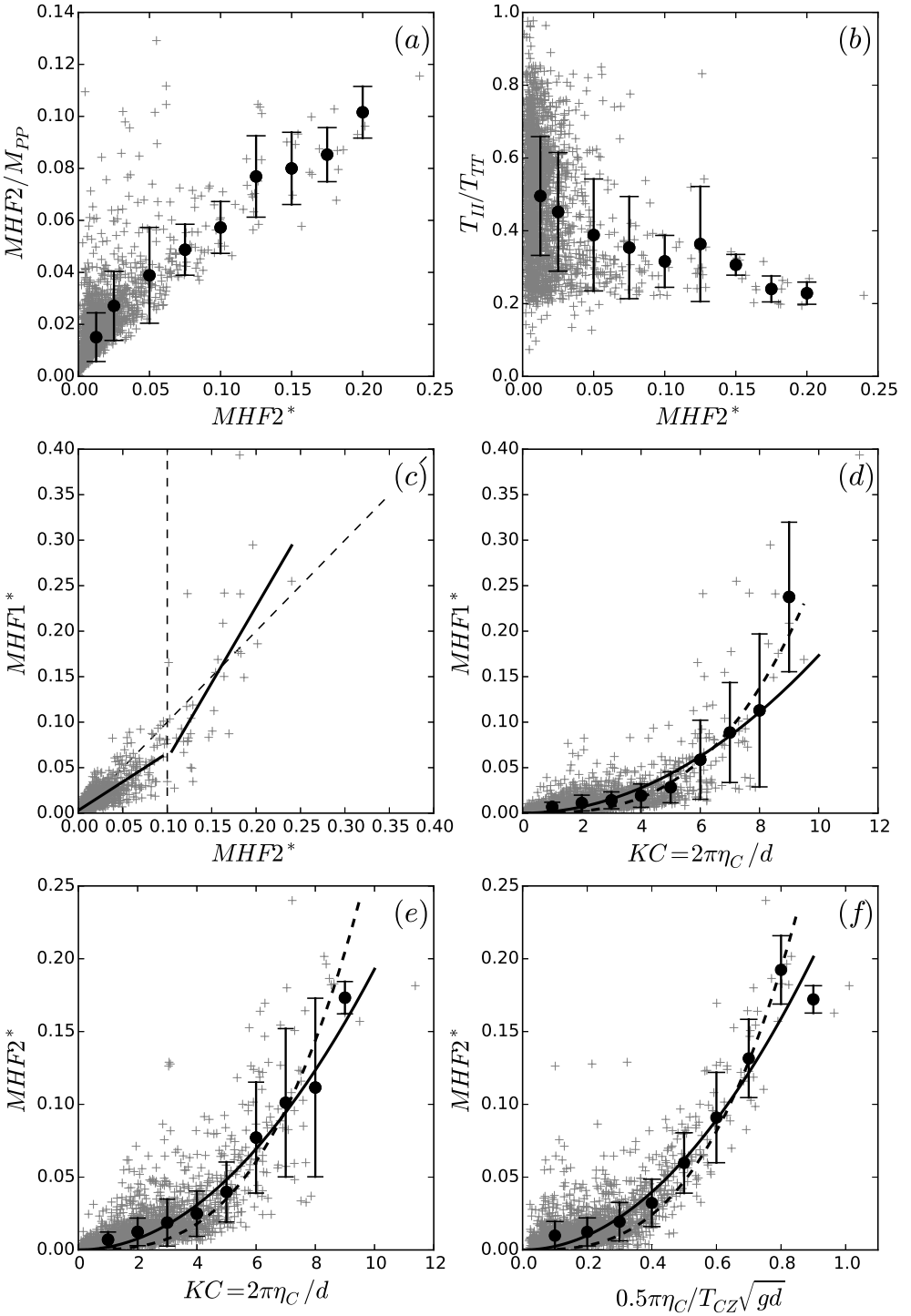


FIGURE 3. High frequency forces components and associated wave parameters in irregular waves. Single events (+) and mean values (•) with bars corresponding to the standard deviation; *(a)* The magnitude of $MHF2^*$ relative to $M^*_{PP}$; *(b)* The timing of $MHF^*$ relative to $T_{TT}$; *(c)* The magnitude of $MHF2^*$ and $MHF1^*$ with fitted linear curves (—); *(d)* $MHF1^*$ as a function of $KC = 2\pi\eta_C/d$ with fitted second (—) and third (– –) order curves; *(e)* $MHF2^*$ as a function of $KC$; and *(f)* $MHF2^*$ as a function of $Fr = 0.5\pi\eta_C/T_{CZ}\sqrt{gd}$.

| | $T_{TT}$ | $2T_{TC}$ | $2T_{CT}$ | $4T_{ZC}$ | $4T_{CZ}$ |
|---|---|---|---|---|---|
| $\alpha_{2,i}x^2$ | 0.57 | 0.80 | 0.43 | 0.89 | 0.33 |
| $\alpha_{3,i}x^3$ | 0.66 | 1.11 | 0.50 | 1.72 | 0.51 |

TABLE 2. Coefficient of variation, $CV$, for fitted second $\alpha_{2,i}x^2$ and third $\alpha_{3,i}x^3$ order curves. For $x = MHF2$ and $Fr = 2\pi\eta_C/T_i\sqrt{gd} > 0.4$ with different wave period definition $T_i$.

$\alpha_3 x^3$, respectively, for $x = KC$, estimated by least squares. For $KC < 5$ the force mean shows an approximately linear behaviour. Around $KC \sim 5$ it appears to be a change to a more rapid growth, and for $KC > 5$ the mean shifts between the higher order curves. A large scatter is observed. For comparison we define the coefficient of variation, CV, by

$$CV = \sqrt{\frac{1}{N}\sum_{i=1}^{N}\left(\frac{y_{i,meas} - y_{i,curve}}{y_{i,curve}}\right)^2}, \tag{3.1}$$

where $y_{i,meas}$ is the measurement, $y_{i,curve}$ the fitted curve and $N$ the number of events. Considering $KC > 5$, $CV = 0.61$ and $0.60$ for the second and third order curves, respectively.

The behaviour of the secondary load cycle, $MHF2^*$ (P2), as a function of $KC$, is shown in figure 3e. Similar to the behaviour of $MHF1^*$, the force mean shows an approximately linear behaviour for $KC < 4$, a change to a more rapid growth for $KC \sim 4-5$, and for $KC > 5$ we observe that the force mean shifts between the two higher order curves. The coefficient of variation are $CV = 0.48$ and $0.55$ for the fitted second and third order curves, respectively, for $KC > 5$.

In figure 3f free surface gravity wave effects on cylinder scale are considered by investigating $MHF2^*$ as a function of the Froude number $Fr$. The secondary load cycle appears close in time with the wave zero-down-crossing, which suggests the use of the speed of the travelling edge of the undisturbed wave to define the wave parameters. Then an improved estimate of the Froude number is suggested by $Fr = 0.5\pi\eta_C/T_{CZ}\sqrt{gd}$. Here, $T_{CZ}$ is the time between the crest and the zero-down-crossing. The measurements are compared to second and third order fitted curves, $\alpha_2 x^2$ and $\alpha_3 x^3$, respectively, for $x = Fr$. We observe the same trends as outlined above for $KC$. A close to linear behaviour when $Fr < 0.3$, a more rapid growth occurs around $Fr \sim 0.3-0.4$, and the force mean shifts from the second to the third order curve for $Fr > 0.4$. The proxy with $Fr$ shows considerable less scatter for the large forces, as compared to the results for $KC$.

All of the periods defined in §2.1 and in figure 1c were analysed with the resulting $CV$ listed in table 2. The best correlation $CV = 0.33$ was found using the time between the crest and the zero-down-crossing, $T_{CZ}$, as shown in figure 3f. Although it is not evident which among the two discussed effects that govern the secondary load cycle, it is clear that the flow velocity is an important parameter. Furthermore, the good correlation with the speed of the travelling edge of the undisturbed wave, indicates that the asymmetry of the wave may be important.

Regarding the peak $MHF1^*$ (P1) the same tendencies are observed, when the function is analysed as a function of $Fr$. The best correlation was again found using the travelling edge of the undisturbed wave to define $Fr$.

## 4. Conclusions

A set of laboratory experiments with a bottom hinged cylinder, exposed to irregular deep water waves, is used to study the strongly nonlinear high frequency forcing with a focus on the secondary load cycle. We consider the forces above a harmonic frequency of $3.5\omega_{TT}$, where $\omega_{TT} = 2\pi/T_{TT}$, and $T_{TT}$ is the trough-to-trough period of the local wave. Two pronounced high frequency force peaks have been identified. The first peak P1 is closely correlated in time with the wave crest. At this time large orbital velocity is present and slamming due to steep and breaking waves may occur. The second peak P2 defines the secondary load cycle. The high frequency force peaks have been studied for 2166 events and related to local wave parameters. . This enables a systematic study of the forces with respect to the two dimensionless parameters, the Keulegan-Carpenter number ($KC$), governing for flow separation, and the Froude number ($Fr$), governing for free surface gravity wave effects. The two high frequency peaks have been investigated by means of regression analysis.

Regarding the secondary load cycle, both $KC$, indicating flow separation effects, and $Fr$, indicating the effect of surface gravity waves, are found to be important. Best correlation is found between the secondary load cycle and $Fr$. The speed of the travelling edge of the undisturbed wave is used to approximate the fluid velocity. A threshold value separating small and large force peaks is found for $KC \sim 4 - 5$ or, alternatively, for $Fr \sim 0.3 - 0.4$, indicating a change in the physical mechanisms that govern the high frequency force. Although it is not clear which of the two effects that dominates, it is clear that the flow velocity is an important parameter for the secondary load cycle. The magnitude of the secondary load cycle is found to be up to $\sim 12\%$ of the peak-to-peak load. The secondary load cycle is found to occur around one quarter of the wave period after the peak of the total load. This generalizes, to the case of irregular waves, previous findings obtained in regular waves.

The study has been carried out with financial support from Stiftelsen Det Norske Veritas, DNV GL and The Research Council of Norway. The technical assistance during the experimental work by Head Engineer Olav Gundersen is gratefully acknowledged.

## REFERENCES

Chaplin, J. R., Rainey, R. C. T. & Yemm, R. W. 1997 Ringing of a vertical cylinder in waves. *Journal of Fluid Mechanics* **350**, 119–147.

Chau, F. P. & Eatock Taylor, R. 1992 Second-order wave diffraction by a vertical cylinder. *Journal of Fluid Mechanics* **240**, 571599.

Chella, M. A., Tørum, A. & Myrhaug, D. 2012 An overview of wave impact forces on offshore wind turbine substructures. *Energy Procedia* **20**, 217–226.

Faltinsen, O. M., Newman, J. N. & Vinje, T. 1995 Nonlinear wave loads on a slender vertical cylinder. *Journal of Fluid Mechanics* **289**, 179–198.

Goda, Y. & Suzuki, Y. 1976 Estimation of incident and reflected waves in random wave experiments. In *Coastal Engineering 1976*, pp. 828–845. American Society of Civil Engineers.

Grue, J. 2002 On four highly nonlinear phenomena in wave theory and marine hydrodynamics. *Applied ocean research* **24** (5), 261–274.

Grue, J., Bjørshol, G. & Strand, Ø. 1993 Higher harmonic wave exciting forces on a vertical cylinder. In *Preprint series. Mechanics and Applied Mathematics, available on http://urn.nb.no/URN:NBN:no-52740*, pp. 1–30. University of Oslo.

Grue, J., Bjørshol, G. & Strand, Ø. 1994 Nonlinear wave loads which may generate 'ringing' responses of offshore structures. In *Ninth International Workshop on Water Waves and Floating Bodies, available on iwwwfb.org.* (ed. M. Ohkusu), pp. 77–81.

Grue, J. & Huseby, M. 2002 Higher-harmonic wave forces and ringing of vertical cylinders. *Applied ocean research* **24** (4), 203–214.

Hasselmann, K., Barnett, T. P., Bouws, E., Carlson, H., Cartwright, D. E., Enke, K., Ewing, J. A., Gienapp, H., Hasselmann, D. E., Kruseman, P., Meerburg, A., Müller, P., Olbers, D. J., Richter, K., Sell, W. & Walden, H. 1973 Measurements of wind-wave growth and swell decay during the joint north sea wave project (jonswap). *Tech. Rep.*. Deutches Hydrographisches Institut.

Kristiansen, T. & Faltinsen, O. M. 2017 Higher harmonic wave loads on a vertical cylinder in finite water depth. *Journal of Fluid Mechanics* **833**, 773–805.

MacCamy, R. C. & Fuchs, R. A. 1954 Wave forces on piles: a diffraction theory. *Tech. Rep.* Technical Memorandum No. 69. Beach Erosion Board.

Malenica, Š. & Molin, B. 1995 Third-harmonic wave diffraction by a vertical cylinder. *Journal of Fluid Mechanics* **302**, 203–229.

Newman, J. N. 1996*a* Nonlinear scattering of long waves by a vertical cylinder. In *Waves and nonlinear processes in hydrodynamics* (ed. John Grue, Bjørn Gjevik & Jan Erik Weber), pp. 91–102. Springer.

Newman, J. N. 1996*b* The second-order wave force on a vertical cylinder. *Journal of Fluid Mechanics* **320**, 417–443.

Paulsen, B. T., Bredmose, H., Bingham, H. B. & Jacobsen, N. G. 2014 Forcing of a bottom-mounted circular cylinder by steep regular water waves at finite depth. *Journal of Fluid Mechanics* **755**, 1–34.

Rainey, R. C. T. 2007 Weak or strong nonlinearity: the vital issue. *Journal of Engineering Mathematics* **58** (1-4), 229–249.

Riise, B. H., Grue, J., Jensen, A. & Johannessen, T. B. 2018 High frequency resonant response of a monopile in irregular deep water waves. *Revised version submitted JFM* .

Sarpkaya, T. 1986 Force on a circular cylinder in viscous oscillatory flow at low keulegancarpenter numbers. *Journal of Fluid Mechanics* **165**, 61–71.

Sheikh, R. & Swan, C. 2005 The interaction between steep waves and a vertical, surface-piercing column. *J. Offshore Mech. Arct. Eng.* **127**, 31–38.

Stansberg, C. T. 1997 Comparing ringing loads from experiments with cylinders of different diameters an empirical study. In *The Eighth Conference on the Behaviour of Offshore Structures (BOSS '97)*, pp. 95–109.

Swan, C. & Sheikh, R. 2015 The interaction between steep waves and a surface-piercing column. *Phil. Trans. R. Soc. A* **373** (2033).

Taylor, R. Eatock & Hung, S. M. 1987 Second order diffraction forces on a vertical cylinder in regular waves. *Applied Ocean Research* **9** (1), 19–30.

Tromans, P., Swan, C. & Masterton, S. 2006 Nonlinear potential flow forcing: the ringing of concrete gravity based structures. *Tech. Rep.* HSE Report 468. Health and Safety Executive, United Kingdom.

Zhen, G., Bingham, H. B., Nicholls-Lee, R. & others 2015 Offshore renewable energy. In *19th International Ship and Offshore Structures Congress*.